all grouped in the high-fugacity regime, below the expected superfluid transition point, confirming that this regime is dominated by superfluidity. Conversely, in the low-fugacity regime the current increases with temperature, corresponding to the channel-dominated regime. The crossover takes place close to the same fugacity for all the gate potentials and is close to the universal transition point for the unitary Fermi gas at the center of the cloud. We expect that the exact location of the crossover as well as the conductance at the minimum depend on the details of the channel geometry, such as its energy-dependent mode spacing. In addition, proximity effects should be reduced at high temperature, and one-dimensional physics could emerge in the QPC, making the results dependent on the length of the contact (*37*). Our setup, allowing for a direct and independent control of the geometry, could be used to investigate such effects in future experiments.

REFERENCES AND NOTES

1. A. J. Leggett, *Quantum Liquids: Bose Condensation and Cooper Pairing in Condensed-Matter Systems* (Oxford Univ. Press, 2006).
2. N. van der Post, E. T. Peters, I. K. Yanson, J. M. van Ruitenbeek, *Phys. Rev. Lett.* **73**, 2611–2613 (1994).
3. E. Scheer, P. Joyez, D. Esteve, C. Urbina, M. H. Devoret, *Phys. Rev. Lett.* **78**, 3535–3538 (1997).
4. O. Fischer, M. Kugler, I. Maggio-Aprile, C. Berthod, C. Renner, *Rev. Mod. Phys.* **79**, 353–419 (2007).
5. W. Zwerger, *The BCS-BEC Crossover and the Unitary Fermi Gas*, vol. 836 (Springer Science & Business Media, 2011).
6. M. W. Zwierlein, J. R. Abo-Shaeer, A. Schirotzek, C. H. Schunck, W. Ketterle, *Nature* **435**, 1047–1051 (2005).
7. S. Nascimbène *et al.*, *Phys. Rev. Lett.* **106**, 215303 (2011).
8. M. J. H. Ku, A. T. Sommer, L. W. Cheuk, M. W. Zwierlein, *Science* **335**, 563–567 (2012).
9. Y. Sagi, T. E. Drake, R. Paudel, R. Chapurin, D. S. Jin, *Phys. Rev. Lett.* **114**, 075301 (2015).
10. C. Cao *et al.*, *Science* **331**, 58–61 (2011).
11. S. Krinner, D. Stadler, D. Husmann, J.-P. Brantut, T. Esslinger, *Nature* **517**, 64–67 (2015).
12. Materials and methods are available as supplementary materials on *Science* Online.
13. R. Labouvie, B. Santra, S. Heun, S. Wimberger, H. Ott, *Phys. Rev. Lett.* **115**, 050601 (2015).
14. A. Schirotzek, Y. I. Shin, C. H. Schunck, W. Ketterle, *Phys. Rev. Lett.* **101**, 140403 (2008).
15. G. Zürn *et al.*, *Phys. Rev. Lett.* **110**, 135301 (2013).
16. D. Stadler, S. Krinner, J. Meineke, J.-P. Brantut, T. Esslinger, *Nature* **491**, 736–739 (2012).
17. G. E. Blonder, M. Tinkham, T. M. Klapwijk, *Phys. Rev. B* **25**, 4515–4532 (1982).
18. D. Averin, A. Bardas, *Phys. Rev. Lett.* **75**, 1831–1834 (1995).
19. J. C. Cuevas, A. Martín-Rodero, A. L. Yeyati, *Phys. Rev. B* **54**, 7366–7379 (1996).
20. C. J. Bolech, T. Giamarchi, *Phys. Rev. Lett.* **92**, 127001 (2004).
21. C. J. Bolech, T. Giamarchi, *Phys. Rev. B* **71**, 024517 (2005).
22. A. M. Zagoskin, *Quantum Theory of Many-Body Systems* (Springer, 1998).
23. A. Kamenev, *Field Theory of Non-Equilibrium Systems* (Cambridge Univ. Press, 2011).
24. O. Avenel, E. Varoquaux, *Phys. Rev. Lett.* **60**, 416–419 (1988).
25. J. C. Davis, R. E. Packard, *Rev. Mod. Phys.* **74**, 741–773 (2002).
26. M. Albiez *et al.*, *Phys. Rev. Lett.* **95**, 010402 (2005).
27. A. Ramanathan *et al.*, *Phys. Rev. Lett.* **106**, 130401 (2011).
28. L. J. LeBlanc *et al.*, *Phys. Rev. Lett.* **106**, 025302 (2011).
29. F. Jendrzejewski *et al.*, *Phys. Rev. Lett.* **113**, 045305 (2014).
30. B. Liu, H. Zhai, S. Zhang, *Phys. Rev. A* **90**, 051602 (2014).
31. T. Giamarchi, *Quantum Physics in One Dimension* (Oxford Univ. Press, 2003).
32. D. L. Maslov, M. Stone, *Phys. Rev. B* **52**, R5539–R5542 (1995).
33. I. Safi, H. J. Schulz, *Phys. Rev. B* **52**, R17040–R17043 (1995).
34. V. V. Ponomarenko, *Phys. Rev. B* **52**, R8666–R8667 (1995).
35. J.-P. Brantut *et al.*, *Science* **342**, 713–715 (2013).
36. T.-L. Ho, *Phys. Rev. Lett.* **92**, 090402 (2004).
37. H. P. Büchler, V. B. Geshkenbein, G. Blatter, *Phys. Rev. Lett.* **92**, 067007 (2004).

ACKNOWLEDGMENTS

We acknowledge discussions with C. Berthod, J. von Delft, E. Demler, C. Grenier, P. Törmä, J. Blatter, and M. Zaccanti. We acknowledge financing from Swiss National Center of Competence in Research Quantum Science and Technology, the European Research Council project Synthetic Quantum Many-Body Systems, the EU Seventh Framework Programme project Simulators and Interfaces with Quantum Systems, Swiss National Science Foundation under division II and the Ambizione program, and the Army Research Office–Multidisciplinary University Research Initiative Non-equilibrium Many-body Dynamics grant (W911NF-14-1-0003). Data are available upon request to T.E.

SUPPLEMENTARY MATERIALS

www.sciencemag.org/content/350/6267/1498/suppl/DC1
Materials and Methods
Figs. S1 to S3
References (*38*–*51*)

5 July 2015; accepted 10 November 2015
10.1126/science.aac9584

ULTRAFAST DYNAMICS

Direct observation of collective modes coupled to molecular orbital–driven charge transfer

Tadahiko Ishikawa,[1]* Stuart A. Hayes,[2,3]* Sercan Keskin,[2,3] Gastón Corthey,[2,3] Masaki Hada,[2,4] Kostyantyn Pichugin,[2] Alexander Marx,[2,3] Julian Hirscht,[2,3] Kenta Shionuma,[1] Ken Onda,[4] Yoichi Okimoto,[1] Shin-ya Koshihara,[1,5] Takashi Yamamoto,[6] Hengbo Cui,[7] Mitsushiro Nomura,[7] Yugo Oshima,[7] Majed Abdel-Jawad,[7] Reizo Kato,[7] R. J. Dwayne Miller[2,3,8]†

Correlated electron systems can undergo ultrafast photoinduced phase transitions involving concerted transformations of electronic and lattice structure. Understanding these phenomena requires identifying the key structural modes that couple to the electronic states. We report the ultrafast photoresponse of the molecular crystal $Me_4P[Pt(dmit)_2]_2$, which exhibits a photoinduced charge transfer similar to transitions between thermally accessible states, and demonstrate how femtosecond electron diffraction can be applied to directly observe the associated molecular motions. Even for such a complex system, the key large-amplitude modes can be identified by eye and involve a dimer expansion and a librational mode. The dynamics are consistent with the time-resolved optical study, revealing how the electronic, molecular, and lattice structures together facilitate ultrafast switching of the state.

The photoexcited states of correlated electron systems often bear strong resemblance to the states reached via thermally induced phase transitions. The phenomenon of a photoinduced phase transition (PIPT) is considered to be an important concept to guide further developments for control of material properties (*1*). However, photoexcitation is intrinsically a far-from-equilibrium process, and new phases or hidden states may also appear (*2*) that differ qualitatively from those observed under equilibrium conditions. Optical pump-probe techniques provide access to the electronic states of the system, but to complete our understanding, it is essential to use an additional structural probe to directly observe the atomic rearrangements involved in propagating the structural transition. This requires the additional step of synchronizing the femtosecond optical excitation laser pulses used to trigger the structure change with a high-brightness femtosecond pulsed x-ray or electron source to observe the atomic motions involved on the relevant time scales. Hard x-ray probes have been shown to be capable of resolving coherent phonons in inorganic materials such as bismuth (*3*, *4*) and in perovskites undergoing PIPTs (*5*); more recently, femtosecond gas-phase x-ray diffraction has been used to provide constraints for a theoretical treatment of a ring-opening reaction (*6*).

[1]Department of Chemistry and Materials Science, Tokyo Institute of Technology, 2-12-1 Oh-okayama, Meguro-ku, Tokyo 152-8551, Japan. [2]Max Planck Institute for the Structure and Dynamics of Matter, Center for Free Electron Laser Science, Luruper Chaussee 149, 22761 Hamburg, Germany. [3]Hamburg Centre for Ultrafast Imaging, University of Hamburg, Luruper Chaussee 149, 22761 Hamburg, Germany. [4]JST-PRESTO, Tokyo Institute of Technology, 4259 Nagatsuta, Midori-ku, Yokohama, Kanagawa 226-8502, Japan. [5]JST-CREST, 4-1-8 Honcho, Kawaguchi, Saitama 332-0012, Japan. [6]Graduate School of Science and Engineering, Ehime University, 2-5 Bunkyo-cho, Matsuyama, Ehime 790-8577, Japan. [7]Condensed Molecular Materials Laboratory, RIKEN, 2-1 Hirosawa, Wako, Saitama 351-0198, Japan. [8]Departments of Chemistry and Physics, University of Toronto, Toronto, Ontario M5S 3H6, Canada.
*These authors contributed equally to this work.
†Corresponding author. E-mail: dwayne.miller@mpsd.mpg.de

Electron sources have also been evolving (*7*–*9*), and femtosecond electron diffraction (FED) has been used to capture a variety of phenomena in inorganic lattices, such as the melting of aluminum (*10*) and suppression of charge-density waves in TaS_2 (*11*). Molecular crystals pose even greater challenges for source brightness because of the increased structural complexity and combination of low damage thresholds, low thermal conductivity, limited reversibility, and large unit cell sizes. Reports of ultrafast diffraction experiments on such systems are scarce, but electron density fluctuations have been observed upon intense nonresonant excitation using laser-based x-ray probes (*12*, *13*). Recent studies of $(EDO\text{-}TTF)_2PF_6$ (EDO-TTF = ethylenedioxytetrathiafulvalene) (*14*) and diarylethene ring-closing reaction dynamics (*15*) have demonstrated the ability of electron probes to observe molecular reactions from well-defined excited states using resonant one-photon excitation of the reactive states. This latter work brings to the forefront the challenge of retrieving the atomic motion from an incomplete set of data.

Here, we followed the electronic and molecular dynamics upon photoexcitation of the correlated electron-molecule-lattice system $Me_4P[Pt(dmit)_2]_2$ (Me_4P = tetramethylphosphonium, dmit = 1,3-dithiol-2-thione-4,5-dithiolate) and directly observed how the cooperative motion of a small

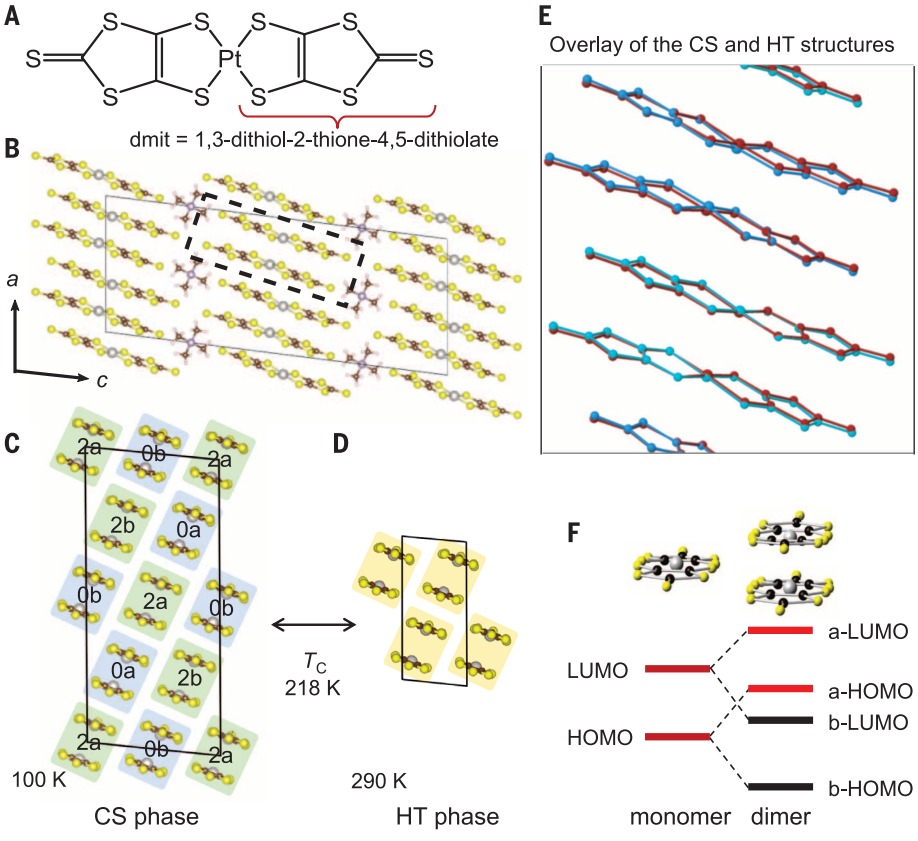

Fig. 1. Chemical and crystal structure. (**A**) Chemical structure of $Pt(dmit)_2$. (**B**) Crystal structure of $Me_4P[Pt(dmit)_2]_2$ viewed along the *b* axis. The dimer unit is surrounded by the thick dashed line. (**C** and **D**) Crystal structure of $Me_4P[Pt(dmit)_2]_2$ viewed along the long molecular axis of $Pt(dmit)_2$ at 100 K [charge-separated (CS) phase] and 290 K [metallic, high-temperature (HT) phase]. 0a, 0b, 2a, and 2b represent the crystallographically independent dimers. (**E**) Overlay of the $Me_4P[Pt(dmit)_2]_2$ molecules in the CS phase (blue for neutral dimer, cyan for divalent dimer) and the HT phase (red). (**F**) Schematic energy level diagram of the molecular orbitals in the $Pt(dmit)_2$ monomer and dimer.

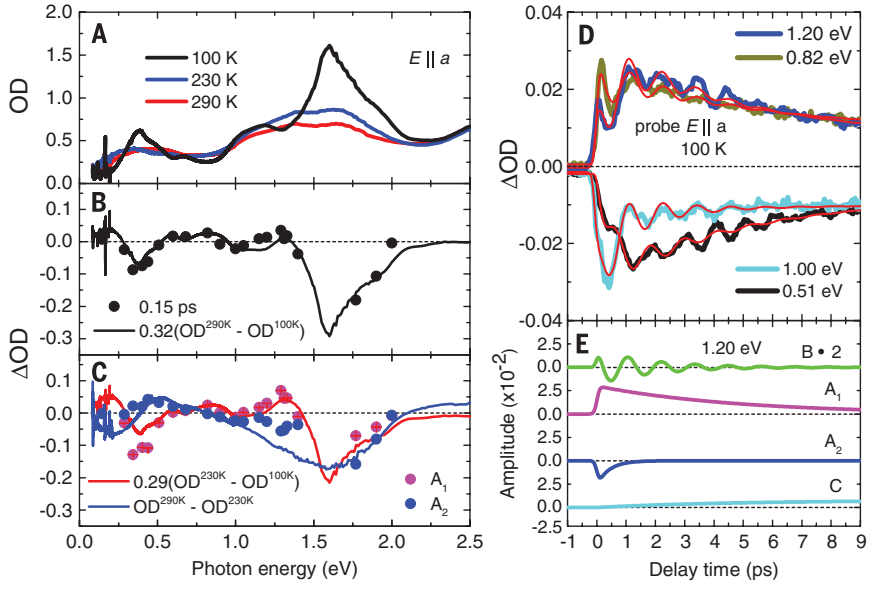

Fig. 2. Ultrafast spectroscopy. (**A**) Temperature dependence of the optical density (OD) spectra of $Me_4P[Pt(dmit)_2]_2$ with polarization along the *a* axis. (**B**) Transient difference in the OD spectrum at 0.15 ps at 100 K (black circles, pump: *E*||*a*, 1.64 × 10^{16} photons/cm^2, 500 Hz; probe: *E*||*a*) and compared with a scaled (0.32) difference spectrum between 290 K (metallic phase) and 100 K (CS phase). (**C**) Spectra of the components of the slow (A_1) and the fast (A_2) relaxation processes from the photo-induced response at 100 K (pink circles, τ = 4.85 ps; blue circles, τ = 0.42 ps); these values are deduced by the fitting procedure (*19*). The red line represents a scaled (0.29) difference OD spectrum between 230 K (metallic phase) and 100 K (CS phase); the blue line represents the difference OD spectrum between 290 and 230 K (both are in the metallic phase). (**D**) Typical temporal profiles of the photoinduced OD change (pump-probe signal; thick colored lines) with various probe photon energies; the fitted curves are shown as thin red lines. (**E**) Temporal profile of the components of the change in OD at 1.2 eV.

number of collective modes leads to transient states similar to those at elevated temperatures, indicating the presence of charge reorganization associated with PIPTs in this type of material. This reduction of a highly multidimensional problem to a few key modes, most strongly coupled to structural transitions (*9*, *14*, *15*), is now directly observable.

$Me_4P[Pt(dmit)_2]_2$ is similar to the compound $Et_2Me_2Sb[Pd(dmit)_2]_2$ (Et_2Me_2Sb = diethyldemethylantimonium), which exhibits a PIPT from a unique charge-separated (CS) phase to an average valence phase, triggered by an intradimer electron excitation (*16*–*18*). $Me_4P[Pt(dmit)_2]_2$ shows a similar CS phase transition, but with a different charge ordering and a higher transition temperature T_c (218 K rather than 70 K), as characterized by resistivity, magnetic susceptibility, and x-ray structural analysis (*19*). The chemical and crystal structures in the high-temperature (HT) phase are shown in Fig. 1, A and B, respectively. The planar $Pt(dmit)_2$ molecules associate into tight dimers and assemble into sheets, which are interleaved with planes of Me_4P cations. Within each $Pt(dmit)_2$ plane, the CS phase transition causes a structural change (Fig. 1, C and D). There are four crystallographically independent dimers in the unit cell of the CS phase, which can be classified into two groups according to the Pt-Pt distances between the molecules: 0a and 0b have a short Pt-Pt spacing of 2.93 Å and are neutral, whereas 2a and 2b are divalent with a charge of –2 and a longer Pt-Pt distance of 3.42 Å. In comparison, the dimers in the HT phase have a charge of –1 and equal Pt-Pt distances, with values of 3.31 Å at 293 K (3.22 Å at 230 K). The neutral and divalent dimers are ordered like a checkerboard in the CS phase, and the breaking of symmetry results in a doubling of the unit cell along both the *a* and *b* axes. A direct comparison between the local structures in the CS and HT phases is shown in Fig. 1E. In the neutral dimer, both the b-HOMO (highest occupied molecular orbital) and b-LUMO (lowest unoccupied molecular orbital) are filled (Fig. 1F), resulting in strong dimerization, but in the anion, the antibonding orbital a-HOMO is also filled, destabilizing the dimer. The relative stability of the CS and HT phases is dependent on a fine balance between this localized effect, interdimer interactions, and long-range Coulomb repulsion (*20*, *21*). The family of dmit salts is therefore considered to be one of the highly correlated electron-molecule-lattice systems.

Figure 2A shows the temperature dependence of the optical density (OD) spectrum of $Me_4P[Pt(dmit)_2]_2$ thin crystals with the polarization of light along the *a* axis. Analogous to the optical conductivity spectra of $Et_2Me_2Sb[Pd(dmit)_2]_2$ (*20*, *22*), we could assign the peak structures in these spectra (*19*) and confirmed that the spectral change was a good representation of the CS phase transition. In addition, the height of the broad peak around 1.5 eV in the HT phase increases with decreasing temperature toward T_c, corresponding to the shortening of the intermolecular distance within the $Pt(dmit)_2$ dimer, which increases the value of the intradimer overlap integral.

We performed time-resolved pump-probe optical spectroscopy and measured the OD changes upon optical excitation using various probe photon energies at 100 K (CS phase). The photon energy of 1.55 eV ($E \| a$) used for the pump matched the intradimer electronic excitation in the neutral dimer. Typical temporal profiles of the pump-probe signal are shown in Fig. 2D along with the fitted curves. The traces also show relaxation-type dynamics and a coherent oscillation. The

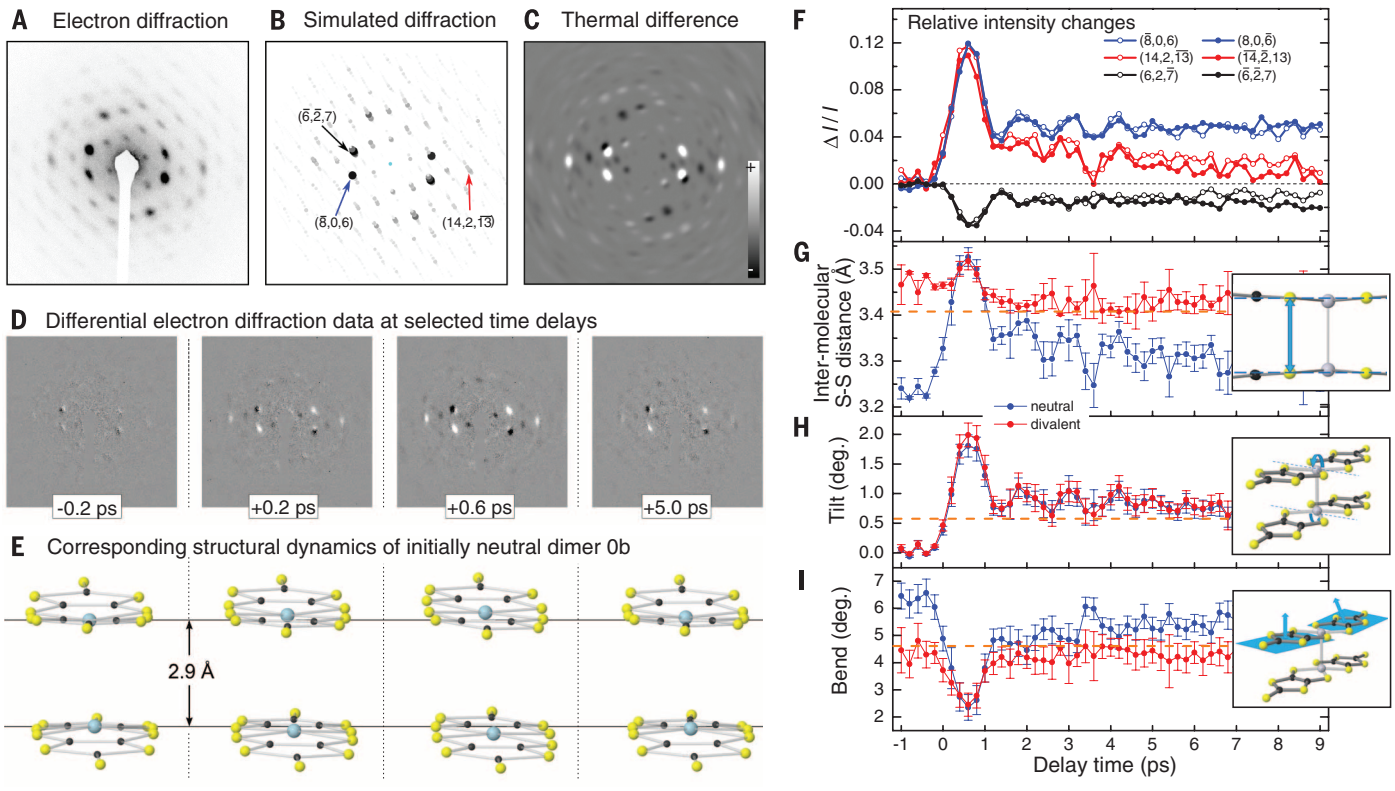

Fig. 3. Femtosecond electron diffraction. (**A**) Experimental diffraction pattern of $Me_4P[Pt(dmit)_2]_2$ at 90 K. (**B**) Simulated diffraction showing the contributions of individual reflections and selected Miller indices. (**C**) Simulated difference pattern for the thermal phase transition: CS phase → HT (metallic) phase, assuming a fixed unit cell. (**D**) Difference FED data [$I^{laser\ on}(t) - I^{laser\ off}$] at the specified time delay, *t*, of the probe electrons with respect to laser excitation. (**E**) A molecular movie of the structural dynamics constructed from the FED data and knowledge of the structures at 100 and 290 K. Snapshots are shown here focusing on one neutral dimer at time points corresponding to the data in (D), with the Pt-Pt distance in the ground state (2.93 Å) shown behind the molecules. (**F**) Temporal profiles of the relative intensity changes of selected diffraction peaks. (**G** to **I**) Dynamics of key structural modes involved in the PIPT for dimers initially neutral (blue) and divalent (red), and compared with the thermal phase transition (dashed orange lines): (G) the intermolecular separation, (H) the tilting of the dimers, and (I) the bend, defined as the angle between the vectors normal to the dmit ligands. Uncertainties were derived from the agreement between models using different input parameters.

temporal dependence of the optical density close to time zero exhibits some variation with energy, especially the data of 1.2 and 0.51 eV compared with the other probe energies, suggesting multiple relaxation pathways. We performed the fitting analysis assuming the summation of two exponential decay–type relaxation processes, one exponentially decayed oscillatory component, and a long-lived component that gradually appears (*19*), as shown in Fig. 2D. Figure 2E shows each fitted component in the 1.2-eV probe data deduced from a global fit to all the data with common relaxation time constants. The two relaxation processes indicate the relaxation of two kinds of photoinduced states. The frequency of the oscillatory component, 0.87 THz, is indicative of a low-energy molecular vibration or lattice phonon mode; this frequency is slightly lower than those observed in other molecular crystals undergoing dimer-Mott (*23*), neutral-ionic (*24*), and spin-crossover photoswitching (*25*, *26*). Figure 2B shows the transient change in the OD spectrum at 0.15 ps after photoexcitation, compared with the difference OD spectrum between 100 and 290 K. The striking similarity suggests the occurrence of a PIPT from the CS phase to a HT-like averaged valence dimer phase. Figure 2C shows the spectra of the photoinduced OD change, which correspond to the slow (τ = 4.85 ps) and the fast (τ = 0.42 ps) relaxation processes, with different spectral shapes. We found that these spectra can be well reproduced by the scaled difference spectra observed at different temperatures for the different phases (red and blue curves in Fig. 2C). The spectrum of the slow relaxation process is similar to that of the thermally induced CS phase transition, whereas the fast relaxation process is similar to the spectral change upon cooling the HT phase. However, the fast relaxation time constant of 0.42 ps is too short to be assigned to a thermal process, and we turn to electron diffraction for more insight into the structural rearrangements accompanying the electronic changes.

The diffraction pattern of thin (<150 nm), crystalline $Me_4P[Pt(dmit)_2]_2$ in the CS phase (90 K), as recorded in our FED instrument, is shown in Fig. 3A. Comparison with the simulated pattern in Fig. 3B reveals that each spot comprises more than one reflection; we attribute this to a combination of the large unit cell size (a = 28.9 Å, b = 12.6 Å, c = 37.4 Å), the finite electron coherence length, and texture of the thin film.

The FED measurements were performed with excitation conditions similar to those of the optical measurements, with excitation of the neutral dimer at a wavelength of 800 nm (1.55 eV) and repetition rate of 250 Hz. The electron probe was generated using a compact electron gun with bunches accelerated to 110 keV, comprising about 4000 electrons and totaling 10^8 electrons per time point measured. The averaged difference images for selected time points are displayed in Fig. 3D. The data immediately preceding excitation (–0.2 ps) are essentially featureless, showing that the structure has relaxed back to the ground state before the excitation pulse arrives at t = 0, whereas the difference images at +0.2 and +0.6 ps show a strong resemblance to the simulated thermal difference pattern (Fig. 3C) (*19*), indicating that the photoinduced structure change is similar to the thermal phase transition, in good agreement with the optical data. After +5.0 ps, the difference pattern retains some similarity to those observed on the subpicosecond time scale, although less pronounced; the dark spots indicate a rise in lattice temperature resulting from redistribution of the absorbed energy into random thermal motion. Quantitative evaluation was performed by integrating the intensities of 40 clearly identifiable spots. A selection of these is shown in Fig. 3F as a function of time. Fitting of the diffraction data using the same functions as for the optical data yielded similar values of the fast time constant of about 0.5 ps, and a frequency of 0.88 THz for the coherent oscillation (*19*), illustrating that the same process is being probed in both the optical and electron diffraction experiments.

A full reconstruction of the atomically resolved dynamics from FED data by direct transfer of the methodology developed for time-resolved crystallography at longer time scales (*27*) would appear to be impossible because of the limited sampling of reciprocal space. Previous studies have approached this problem by searching expected reaction coordinates for maximum correlation between theory and experiment (*14*, *15*); instead, we refined individual atom positions by defining a minimization function that combines the experimental FED data with the known structures involved in the thermal phase transition and using penalty functions to bias the optimization toward chemically reasonable structures (*19*). The additional information stabilized the refinement and enabled us to optimize all atomic coordinates in the asymmetric unit comprising 103 atoms. In this way we could avoid assumptions of specific reaction modes, making the discovery of unexpected structures possible. Movies S1 and S2 show the structural dynamics as observed from different perspectives; snapshots showing one neutral dimer are displayed in Fig. 3E. Three distinct motions can be easily identified from the molecular movies: an expansion of the intermolecular distance in the neutral dimer, flattening of the molecules, and a libration or tilting of all dimers in unison. To discuss the structural dynamics quantitatively, we parameterized these motions along with three additional collective variables: a rotational motion perpendicular to the tilt, and two orthogonal intradimer sliding motions (fig. S5). The temporal profiles of the intermolecular distance, monomer tilt, and bend motions are shown in Fig. 3, G to I.

These photoinduced dynamics can be compared with the structure changes associated with the thermal phase transition, which are represented by the orange dashed lines in Fig. 3, G to I; they can also be understood in terms of the optical data as summarized in Fig. 4. Photoexcitation of the neutral dimer initiates a rapid expansion of the intermolecular distance, which acts as a photoswitch and within 0.5 ps produces a state that is similar to the HT phase at 290 K (Fig. 4B), as seen by the convergence of the parameter values for the neutral and divalent dimers. This is accompanied by a tilting of all dimers, which should be identified as a librational mode of the lattice, because there is no discrimination between the neutral and divalent species. The initial excitation also flattens the $Pt(dmit)_2$ monomers, predominantly in the neutral species. However, this state is unstable and relaxes back to an intermediate structure, with τ = 0.42 ps—a relaxation that appears optically similar to a cooling from 290 K to 230 K (Fig. 4C). The associated structural relaxation is a partial reversal of the initial structure change, with a contraction of the neutral dimer to give an intermolecular distance just below the value of the HT phase at 230 K and a smaller contraction of the divalent dimers to produce a metastable state that is similar to the HT phase. The tilting mode similarly relaxes back to an intermediate value. These fast dynamics are accompanied by a pronounced oscillation with a frequency of 0.87 THz that persists for a few picoseconds, as clearly seen in both the optical and diffraction data. The structural origin deduced from the diffraction studies is related to the lattice libration of the tilting mode (Fig. 4D), as revealed by the especially pronounced oscillation in this degree of freedom (Fig. 3H).

The large unit cell of this system demonstrates that FED can provide insight into complex problems in ultrafast materials science, and suggests the possibility of extension to even larger systems. The method used in the structure determination provides a general approach to FED data analysis that can be applied to any system with a known initial ground-state structure. This approach provides a new window on directly

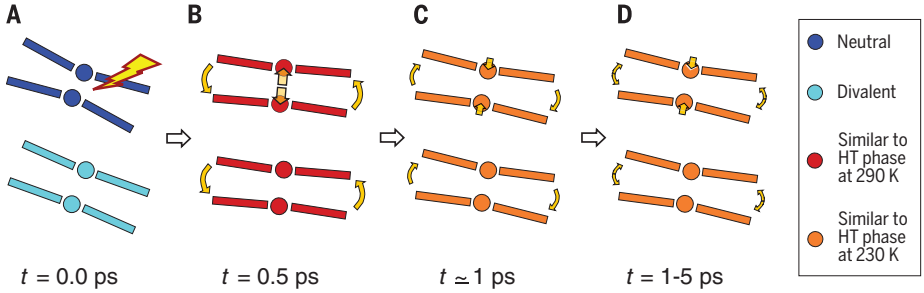

Fig. 4. Summary of the ultrafast dynamics. (**A** to **D**)The solid circles depict Pt atoms; the solid bars are dmit ligands. The color scheme represents the spectroscopic similarity of the excited states to those at thermal equilibrium. The arrows indicate displacements along large-amplitude modes observed by FED.

observing the key modes involved in propagating structural transitions and the enormous simplification this affords in understanding the structural dynamics of complex systems.

REFERENCES AND NOTES

1. K. Nasu, Ed., *Photoinduced Phase Transitions* (World Scientific, 2004).
2. H. Ichikawa *et al.*, *Nat. Mater.* **10**, 101–105 (2011).
3. K. Sokolowski-Tinten *et al.*, *Nature* **422**, 287–289 (2003).
4. D. M. Fritz *et al.*, *Science* **315**, 633–636 (2007).
5. P. Beaud *et al.*, *Nat. Mater.* **13**, 923–927 (2014).
6. M. P. Minitti *et al.*, *Phys. Rev. Lett.* **114**, 255501 (2015).
7. J. C. Williamson, J. Cao, H. Ihee, H. Frey, A. H. Zewail, *Nature* **386**, 159–162 (1997).
8. A. H. Zewail, *Science* **328**, 187–193 (2010).
9. R. J. D. Miller, *Annu. Rev. Phys. Chem.* **65**, 583–604 (2014).
10. B. J. Siwick, J. R. Dwyer, R. E. Jordan, R. J. D. Miller, *Science* **302**, 1382–1385 (2003).
11. M. Eichberger *et al.*, *Nature* **468**, 799–802 (2010).
12. M. Braun *et al.*, *Phys. Rev. Lett.* **98**, 248301 (2007).
13. T. Elsaesser, M. Woerner, *J. Chem. Phys.* **140**, 020901 (2014).
14. M. Gao *et al.*, *Nature* **496**, 343–346 (2013).
15. H. Jean-Ruel *et al.*, *J. Phys. Chem. B* **117**, 15894–15902 (2013).
16. T. Ishikawa *et al.*, *Phys. Rev. B* **80**, 115108 (2009).
17. N. Fukazawa *et al.*, *J. Phys. Chem. C* **117**, 13187–13196 (2013).
18. K. Nishioka, K. Yonemitsu, *J. Phys. Soc. Jpn.* **82**, 094716 (2013).
19. See supplementary materials on *Science* Online.
20. H. Tajima *et al.*, *Solid State Commun.* **79**, 337–341 (1991).
21. M. Tamura, R. Kato, *Chem. Phys. Lett.* **387**, 448–452 (2004).
22. M. Tamura *et al.*, *Chem. Phys. Lett.* **411**, 133–137 (2005).
23. Y. Kawakami *et al.*, *Phys. Rev. Lett.* **103**, 066403 (2009).
24. H. Okamoto *et al.*, *Phys. Rev. B* **70**, 165202 (2004).
25. C. Consani *et al.*, *Angew. Chem. Int. Ed.* **48**, 7184–7187 (2009).
26. M. Cammarata *et al.*, *Phys. Rev. Lett.* **113**, 227402 (2014).
27. I. I. Vorontsov *et al.*, *J. Am. Chem. Soc.* **131**, 6566–6573 (2009).

ACKNOWLEDGMENTS

We thank G. Sciaini and G. Moriena for help constructing the FED apparatus; W. Kazub, M. Lorenc, and A. Moreac for their help in the early stage of the optical study; and T. Tsumuraya for information concerning the band calculation. The electron diffraction work was funded by the Max Planck Society in collaboration with the Centre for Free Electron Laser Science and the Hamburg Centre for Ultrafast Imaging. This work was also partially supported by Grants-in-Aid for Scientific Research (A) (no. 15H02103) from the Ministry of Education, Culture, Supports, Science, and Technology of Japan, and CREST, JST. G.C. thanks the Alexander von Humboldt Foundation for support. M.H. acknowledges the Japan Science Technology Agency (JST), PRESTO, for funding the project "Molecular technology and creation of new functions." The authors declare no conflicts of interest.

SUPPLEMENTARY MATERIALS

www.sciencemag.org/content/350/6267/1501/suppl/DC1
Materials and Methods
Figs. S1 to S24
Tables S1 to S4
Movies S1 and S2
References (*28*–*32*)

14 April 2015; accepted 6 November 2015
10.1126/science.aab3480

QUANTUM SIMULATION

Josephson effect in fermionic superfluids across the BEC-BCS crossover

Giacomo Valtolina,[1,2,3] Alessia Burchianti,[1,2] Andrea Amico,[1,2,4] Elettra Neri,[1,2,4] Klejdja Xhani,[1,2] Jorge Amin Seman,[1]* Andrea Trombettoni,[5] Augusto Smerzi,[1,2,6] Matteo Zaccanti,[1,2] Massimo Inguscio,[2,4,7] Giacomo Roati[1,2]†

The Josephson effect is a macroscopic quantum phenomenon that reveals the broken symmetry associated with any superfluid state. Here we report on the observation of the Josephson effect between two fermionic superfluids coupled through a thin tunneling barrier. We show that the relative population and phase are canonically conjugate dynamical variables throughout the crossover from the molecular Bose-Einstein condensate (BEC) to the Bardeen-Cooper-Schrieffer (BCS) superfluid regime. For larger initial excitations from equilibrium, the dynamics of the superfluids become dissipative, which we ascribe to the propagation of vortices through the superfluid bulk. Our results highlight the robust nature of resonant superfluids.

The Josephson effect (*1*) allows extraction of the most elusive part of the superfluid order parameter, the phase, through a measurable quantity, a particle current (*2*). Furthermore, Josephson dynamics provide fundamental insights into the microscopic properties of superfluids and their robustness against dissipative phenomena (*3*). Since its discovery, the Josephson effect has been demonstrated in a variety of fermionic and bosonic systems (*3*–*12*). However, it has so far eluded observation in Bose-Einstein condensate (BEC)–Bardeen-Cooper-Schrieffer (BCS) crossover superfluids (*13*, *14*) realized by ultracold Fermi gas mixtures close to a Feshbach resonance (*15*, *16*). These systems encompass the two paradigmatic aspects of superfluidity within a single framework: Bose-Einstein condensation of tightly bound molecules and BCS superfluidity of long-range fermion pairs (*13*). Moreover, in the resonant regime, where the pair size is comparable to the interparticle spacing, they show universal properties, exhibiting similarities to other exotic strongly correlated fermionic superfluids, from cuprate superconductors to nuclear and quark matter (*17*, *18*). Here we report on the observation of the Josephson effect in ultracold gases of ^{6}Li atom pairs across the BEC-BCS crossover. Our Josephson junction consists of two superfluid reservoirs, weakly coupled through a thin tunneling barrier. For all interaction regimes, we detected coherent oscillations of both the pair population imbalance $\Delta N = N_L - N_R$ and the

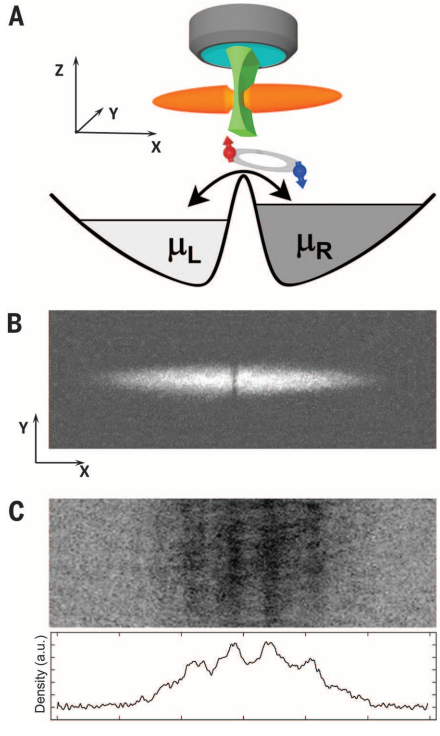

Fig. 1. Josephson junction between two ultracold fermionic superfluids. (**A**) Sketch of the experimental apparatus. The junction is realized by bisecting trapped superfluids of ^{6}Li atom pairs with an optical barrier that is only a few times wider than the correlation length of the system. Red and blue arrows indicate the two different spin components forming the fermionic pairs. The dynamics are monitored by recording the number imbalance and relative phase between the two reservoirs via in situ (**B**) and time-of-flight (**C**) imaging, respectively (a.u., arbitrary units).

[1]Istituto Nazionale di Ottica del Consiglio Nazionale delle Ricerche (CNR), 50019 Sesto Fiorentino, Italy. [2]European Laboratory for Nonlinear Spectroscopy (LENS), 50019 Sesto Fiorentino, Italy. [3]Faculty of Mathematic and Natural Sciences, Scuola Normale Superiore, 56126 Pisa, Italy. [4]Department of Physics and Astronomy, University of Florence, 50019 Sesto Fiorentino, Italy. [5]Istituto Officina dei Materiali del CNR and Scuola Internazionale Superiore di Studi Avanzati, I-34136 Trieste, Italy. [6]Quantum Science and Technology in Arcetri, I-50125 Firenze, Italy. [7]Istituto Nazionale di Ricerca Metrologica, 10135 Torino, Italy.
*Present address: Instituto de Fisica, Universidad Nacional Autonoma de Mexico, Apartado Postal 20-364, 01000 Mexico Distrito Federal, Mexico. †Corresponding author. E-mail: giacomo.roati@ino.it